Shaping of ceria-based single solid oxide cells combining tape-casting, screen-printing and infiltration

Laura Guesnet, Jean-Marc. Bassat, Jean-Claude Grenier, Thierry Chartier, Pierre-Marie Geffroy

Shaping of ceria-based single Solid Oxide Cells combining tape-casting, screen-printing and infiltration

L. Guesnet[1,2], J.-M. Bassat[1], J.-C. Grenier[1], T. Chartier[2] and P.-M. Geffroy[2,*]

[1] CNRS, Univ. Bordeaux, Bordeaux INP, ICMCB, UMR 5026, F-33600 PESSAC Cedex, France

[2] CNRS, Institut de Recherche sur les Céramiques (IRCER), UMR 7315, Centre Européen de la Céramique, 12 rue Atlantis, 87068 LIMOGES Cedex, France

* Corresponding author

Dr. Pierre-Marie GEFFROY,
IRCER, CNRS UMR 7315, 12 Rue Atlantis 87068 Limoges,
Tel.: +33 587 502 353,
Fax: +33 587 502 304,
E-mail: pierre-marie.geffroy@unilim.fr

Abstract

This study describes the development of a shaping process involving GDC10 ($Ce_{0.9}Gd_{0.1}O_{1.95}$) as an electrolyte for Solid Oxide Cells operating at low temperature (500-600°C). The goal is to build a single cell of porous/dense/porous GDC10 layers while adapting the porous layer thicknesses, which are infiltrated by catalysts to prepare efficient GDC-base composites. Two shaping processes were used to make the cell. The first process is die pressing of the electrolyte powder followed by the infiltration of a screen-printed porous backbone. The second shaping process consists of preparing a porous/dense/porous (30 µm/≈ 400 µm/30 µm) cell in a single step by combining tape-casting and screen-printing processes followed by the infiltration of the previous catalyst.

Keywords: Ceria, tape casting, infiltration method, Solid Oxide Cells

1) Introduction

Yttria-stabilized zirconia (YSZ) is commonly used as the electrolyte of conventional Solid Oxide Fuel Cells (SOFCs) due to its high ionic conductivity and good stability in reducing and oxidizing atmospheres [1]. However, conventional SOFCs operate at high temperature (> 800°C) [2], and the main critical challenges for the commercial development of SOCs (Solid Oxide Cells) (including SOFCs and Solid Oxide Electrolysis Cells, SOECs) is their long-term chemical stability [3] at these operating temperatures. Indeed, several degradation mechanisms have been reported after a long operating period, which can also depend on whether the SOFC or SOEC modes are considered [4]–[7]. For example, considering the usual oxygen electrode (*i.e.,* $La_{0.6}Sr_{0.4}$ $Co_{0.2}Fe_{0.8}O_{3-\delta}$ (LSCF) composition), a diffusion of strontium towards the electrolyte generally occurs at high temperature [8]. In addition, Co element is volatile during high-temperature sintering, and its cost is relatively high [9]. Moreover, in the SOEC mode, a demixing of the air electrode material and the formation of oxygen bubbles at the grain boundaries are often observed [5]. The possible reversible use of SOCs at reduced operating temperature must also be carefully considered [10].

An efficient route to prevent the cation diffusion is to coat the YSZ electrolyte with an ionic conducting barrier layer, typically gadolinium-doped ceria, *i.e*., GDC10 and GDC20 for $Ce_{0.9}Gd_{0.1}O_{1.95}$ and $Ce_{0.8}Gd_{0.2}O_{1.9}$, respectively. However, to fully densify this thin GDC layer, temperatures as high as 1400°C must be used [11], [12]. The last step of this process is the preparation of the oxygen electrode side by screen-printing a porous LSCF layer and a subsequent heat treatment at T $\sim$ 1150°C [13].

Finally, the manufacturing of SOCs requires treatments at high temperature, which is a detrimental point to maintain an efficient electrode microstructure with the large specific surface area and appropriate porosity. Moreover, as described above, operating the cell at high temperature increases its thermo-chemical degradation.

A method to limit such degradation effects is to operate the SOCs at reduced temperature, *i.e.,* 500 < T°C < 600. This temperature range also enables the use of conventional low-cost stainless-steel materials for the interconnects. For this purpose, GDC10(20) is an appropriate electrolyte due to its high ionic conductivity in this low temperature range [14], [15]. However, at such low temperatures, the electro-activity performances of both air and fuel electrodes must be increased. Another important point to consider is the thermo-mechanical compatibility between electrolyte and electrodes.

The surface modification of porous electrodes through the infiltration route of catalysts is effective to address these two points. Thus, the active catalysts are generally infiltrated as a solution into a porous backbone of the ionic conductor (while the reverse process, *i.e.,* infiltration of an ionic conductor in a backbone with MIEC properties, is also possible) to prepare an efficient composite, as developed by several groups in recent years [16], [17]. Indeed, the ionic conductor used as a backbone generally has higher ionic conductivity than electrode materials, especially on the air electrode side [17]. Thus, the efficiency of such nano-structured electrodes is improved due to enlarged surface areas, but thermo-mechanical issues may occur [18]. This fabrication process usually requires lower temperatures than the value needed to sinter a screen-printed electrode, which limits the problems of cationic inter-diffusion among various cell elements.

According to recent publications, efficient composite electrodes can be prepared by impregnating electro-catalysts in a thin and porous GDC backbone. Prior to infiltration, the backbone is screen-printed on a dense electrolyte, which is usually YSZ [19], [20] or GDC [21], and subsequently sintered at high temperature.

Regarding the above issues, this work focuses on the use of the same material for both electrolyte and backbone, *i.e.,* GDC. The main goal is to make a single cell of porous/dense/porous GDC layers, which are subsequently infiltrated by catalysts. In the first step, symmetrical cells are considered, and the porous parts are infiltrated to prepare Pr_6O_{11}/GDC composite oxygen electrodes. Note that GDC10 was used in this study instead of GDC20 only because of the availability of the powder with appropriate characteristics; however, the GDC20 composition is also convenient. In the second step, an innovative process combining tape-casting/screen-printing and infiltration using GDC as a unique electrolyte is developed. The main advantages of this process combining tape casting and screen - printing are the shaping of cells in one-step, the accurate thickness control and the interface quality between electrolyte and electrodes. This shaping process allows preparing an asymmetric architecture including a thin dense electrolyte and a thick porous support, likely corresponding to the best compromise between good mechanical properties and high electrochemical performances of the cells. In addition, only one high temperature sintering is required, which allows reducing costs in terms of electrical energy.

The Pr_6O_{11}/GDC composites were selected based on our own experience on the corresponding electrodes deposited on YSZ electrolytes, which yield excellent electrochemical performances at low temperature, *i.e.,* 600°C. Indeed, the simple oxide Pr_6O_{11} is an excellent electro-catalyst for the oxygen reduction reaction despite its quite poor electronic conductivity [22]. For instance, at 600°C the oxygen diffusion coefficient value is as high as 3.4×10^{-8} $cm^2.s^{-1}$, and that of the surface exchange coefficient is 5.4×10^{-7} $cm.s^{-1}$, which are in agreement with excellent electro-catalytic properties. The development of different fabrication steps and their optimization are detailed. Two different and low-cost cell shaping processes are necessary before reaching the goal. These processes are described with the corresponding electrochemical characterization. In the second step, the preparation of the GDC-based porous layer support (thickness approximately 200 µm)/dense (thickness approximately 10-20 µm)/porous (thickness approximately 20-30 µm) will be described, which paves the way to prepare a single cell.

To the best of our knowledge, this process, which is dedicated to the shaping of Solid Oxide Cells, is completely innovative.

2) Experimental

2.1.) Preparation of GDC-based solid oxide symmetrical cells

Two manufacturing routes are successively described in the following sections. The first one is die pressing associated with screen-printing (2.1.1). Die pressing was used to prepare a *reference sample*. The second route is tape-casting with the aim to obtain an optimized thin electrolyte in terms of ionic conductivity (2.1.2). The parameters of the tape casting process were optimized to obtain the best electrochemical performances of this electrolyte, close to those obtained for the die pressed pellet.

Figure 1 shows the two shaping processes in this work: 1) Pressing/Screen-printing/Infiltration and 2) Tape-casting/Infiltration.

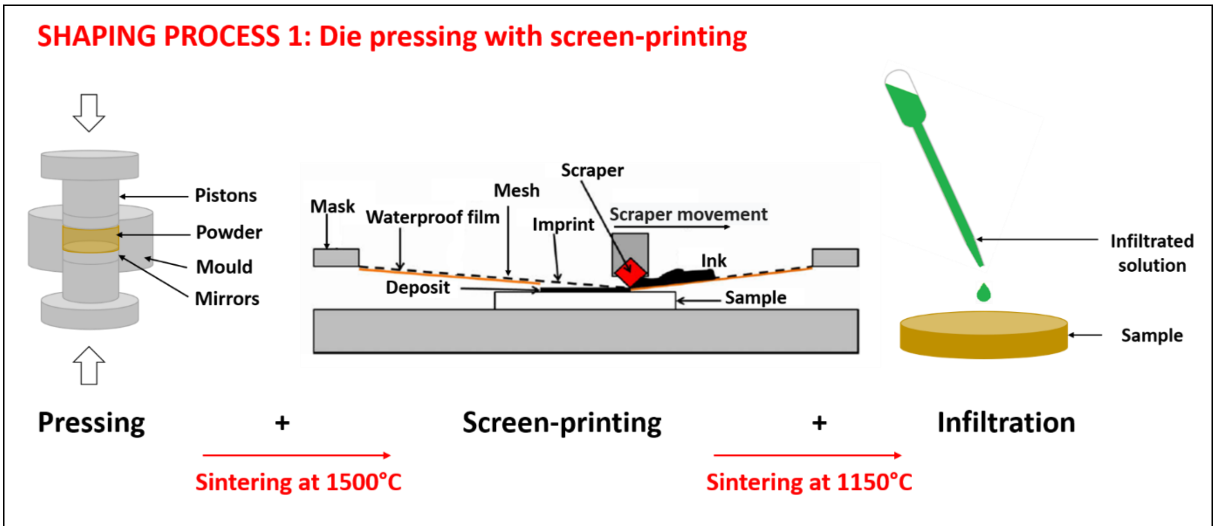

a)

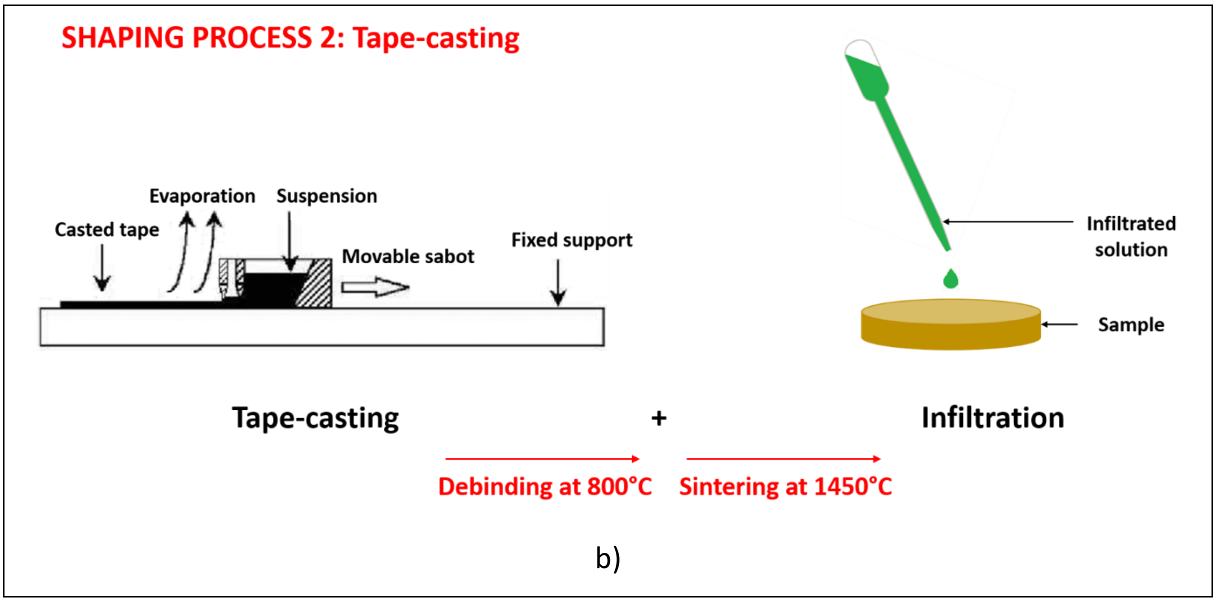

Figure 1: Schemes of the shaping processes: a) Shaping process 1 (pressing/screen-printing/infiltration and b) Shaping process 2 (tape-casting/infiltration)

2.1.1) Cell shaping by die pressing associated to screen-printing

The selected solid electrolyte was gadolinium-doped ceria GDC10 ($Ce_{0.9}Gd_{0.1}O_{2-\delta}$) due to its high ionic conductivity (σ_i = 0.0095 $S.cm^{-1}$ at 500°C) [14]. A commercial powder (provided by Solvay) was uniaxially pressed to obtain a green pellet with 25-mm diameter and 0.8-mm thickness before sintering. The pellets were sintered at 1500°C in 3 h to reach a relative density of approximately 95% (Archimedes' method). Subsequently, a porous skeleton GDC10 and an $LaNi_{0.6}Fe_{0.4}O_{3-\delta}$ (LNF) collecting layer [23] were successively screen-printed on the dense pellet. The diameters of the backbone and collecting layer were 16 mm. The backbone was 30 µm thick, and the collecting layer was 10 µm thick. In each case, the prepared inks contained a pore-forming agent ("Carbon Super P", TIMCAL, France, mean particle size=1.6 µm). To dry each layer, a heat gun (T ~ 200°C) was used.

Then, the backbone and current collecting layer were co-sintered at 1150°C for 1 h in air (Figure 2).

In the third step, the catalyst was injected into the backbone.

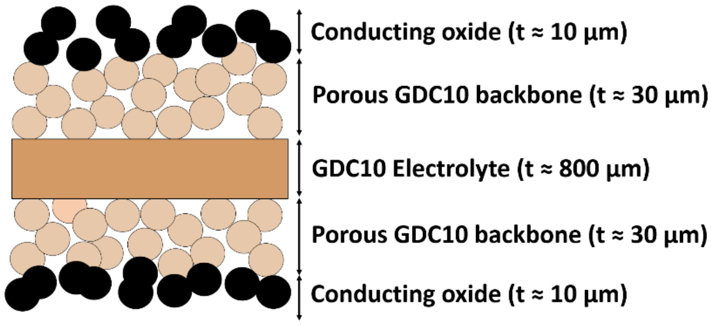

Figure 2: Scheme of a symmetrical cell (oxygen side) before infiltration

In the final step, the symmetrical cells were heat-treated at 600°C under air flow to obtain the required catalyst.

2.1.2) Cell shaping by tape casting (GDC10-based porous/dense/porous)

The tape casting process enables us to manufacture a thin GDC10 porous/dense/porous support *in a single step* with a given porosity of the backbone, which can be controlled by the amount of pore-forming agent in the slurry and the sintering conditions. Indeed, the sintering temperature must be optimized to simultaneously maintain a high porosity ratio, sufficient mechanical cohesion of the porous backbone and a relative density of the electrolyte above 95%.

Elaboration of green ceria tapes

The suspension for the tape casting process was of the GDC10 powder, a solvent, and organic additives (dispersing agent, plasticizer and binder) to obtain homogeneous green tapes without cracks, which can be easily handled. The ceria powder was milled by planetary milling for 5 h in the azeotropic mixture (60% vol. MEK/40% vol. ethanol) with the addition of the dispersant agent (phosphate ester) and zirconia or alumina balls. The addition of the dispersant agent led to a good dispersion of the GDC10 particles in the solvent. Then, a binder (polyvinyl butyral, PVB B90, Brenntag or polymethacrylate D51/07, Degussa) and a plasticizer (dibutyl phthalate, DBP) were added to the slurry, with a subsequent low-speed ball-milling of 12 h. The addition of a binder and a plasticizer yielded cohesive and flexible green tapes after drying [24]–[26]. The viscosity of the suspension containing 17 vol% ceria powder was close to 1 Pa.s^{-1}, which was adapted to the casting of thin sheets (*i.e.,* 50 µm in thickness for the porous layers). In order to elaborate porous electrode layers, carbon particles of approximately 1.6-µm diameter were introduced as the pore-forming agent. Approximately 80 vol. % of carbon pore former with respect to GDC10 powder was added in the suspension. The obtained green tapes, containing or not pore forming agent, with a thickness of approximately 100 µm for the dense layer were punched into 25-mm-diameter disks.

Elaboration of porous/dense/porous stacks of disks

Then, according to the desired sequence (porous/dense/porous) and thickness, stacks of disks with and without the pore-forming agent were laminated at 110°C under 54 MPa to obtain the required total thickness of approximately 400 µm. The debinding of green stacks were performed at 800°C during 2 h in air to remove organic additives and finally sintered at high temperature (approximately 1500°C).

2.1.3) Infiltration of porous electrodes

On the oxygen side, the selected catalyst was Pr_6O_{11} [22]. Therefore, a concentrated solution of praseodymium nitrate was infiltrated (under vacuum) in the porous GDC layer until the mass ratio of infiltrated material to backbone material was approximately 30 wt. % of the porous layer.

2.2) Chemical and physico-chemical analyses of GDC10 electrolytes

Several physico-chemical analyses were performed on the samples prepared by tape casting and on the organic additives for the suspension to help understanding the origin of possible differences in electrochemical performances compared to a pressed electrolyte.

2.2.1) ICP analyses

The ICP analysis (ICP/OEC, Varian ICP/OEC 720 ES) enables us to determine the qualitative and quantitative amounts of elements in the solution. The suspension in the tape-casting process includes many organic additives (*i.e.,* dispersant, binder, plasticizer), all of which can introduce pollution, which can be detrimental to the electrochemical performances as later discussed in the paper.

Based on preliminary experiments performed using an X (Castaing) micro-probe (line scanning) on tape-casted GDC10 layers, the following elements were analysed: Na, Al, Si, K and P. Al and Si should come from the milling step, while Na, K and P can be introduced *via* the organic additives of the tape-casting suspensions.

The chemical analysis of binders was performed on ashes obtained after the pyrolysis of binders at 400°C for 1 h to improve the detection limit of possible impurities in the binders.

2.2.2) Auger analyses

Auger analysis (nanoprobe Auger Phi 710, Feder) provides high-resolution images of a sample area and helps us determine the local elemental chemical composition (the surface area of analysis is approximately 0.05-0.15 µm²). Moreover, it is possible to obtain the depth profile of each element concentration.

2.3) Electrochemical Impedance Spectroscopy (EIS) measurements on symmetrical cells

Electrochemical impedance spectroscopy was used to characterize the GDC10 electrolytes and symmetrical cells electrode/GDC10/electrode. For the measurements, the electrolytes were simply painted with platinum paste, while the symmetrical cells (including the current-collecting layer) were placed between two gold grids supported by channelled alumina ceramics. In both cases, a weight was applied to improve the current collection. The impedance diagrams were recorded every 50°C between 200°C and 800°C in the frequency range from 1 MHz to 0.1 Hz. The series and polarization resistances (R_s and R_p, respectively) were calculated from the impedance diagrams, which were fitted using an equivalent circuit made of a series resistance and R-CPE equivalent elements. A detailed description of the fitting process was given in a previous work, e.g., [27].

The series resistance R_s primarily characterizes the total electrical conductivity of the electrolyte (which includes the bulk and grain boundary contributions) according to relation (1):

$$\sigma_T = \frac{1}{R_s} \cdot \frac{t}{S} \qquad (1)$$

where t and S are the thickness and surface of the pellet, respectively.

3) Results and discussion

This section concerns the development of a GDC10-based porous/dense/porous cell, which was made in one step (tape casting) followed by the infiltration of Pr_6O_{11} catalyst in the porous layers of this architecture (namely, “symmetrical SOC”). Finally, this cell is characterized by electrochemical impedance spectroscopy (EIS) to show the following:

- the sintered dense electrolyte made by tape casting has an ionic conductivity close to the standard value of the literature for GDC10 (this one being close to the *reference cell* one shaped by die pressing in this work, see below).

- the electrochemical measurements on the infiltrated (Pr_6O_{11}) symmetrical SOC show similar polarisation resistance values to those that we previously measured ($R_p \approx 30$ mΩ cm² at 600°C [22]).

For this purpose, our strategy involves two successive steps: 1) optimization of the shaping of the dense part of the architecture by tape-casting and characterization of its ionic conductivity by EIS using Pt electrodes and 2) manufacture of the porous/dense/porous architecture in one step by optimized tape casting, infiltration of the Pr_6O_{11} catalyst and EIS characterization of the symmetrical SOC using a current-collecting layer (LNF).

Figure 3 is an example of a tape-casted cell architecture prior to the infiltration step. The relative density of the electrolyte is approximately 98%, while the skeleton porosity is 38%, which is only slightly lower than that of the screen-printed electrode (45%).

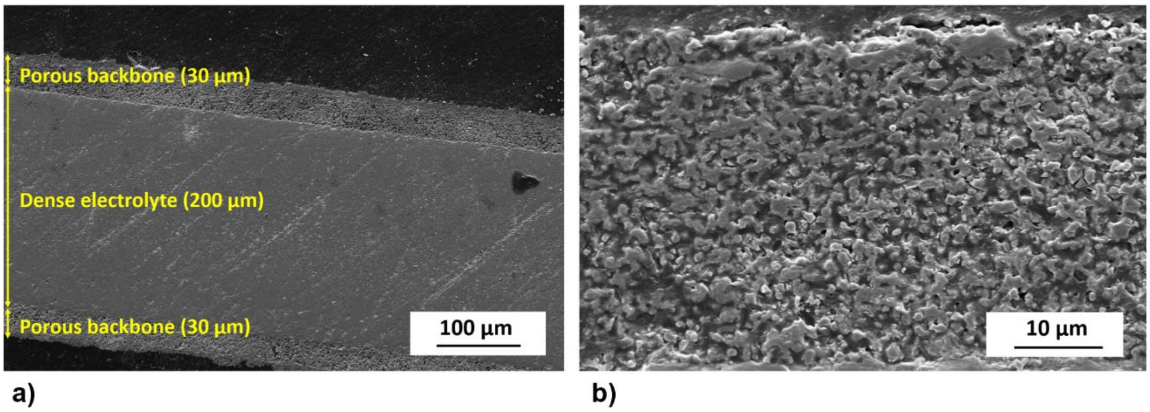

Figure 3: a) Porous/dense/porous sample manufactured by tape-casting/lamination/sintering before infiltration and b) zoom-in view of the porous backbone layer (38% porosity)

The final step was the infiltration of the porous layers by praseodymium nitrate, as described later.

3.1) Ionic conductivity of the GDC10 electrolyte shaped by different processes

The shaping process affects the electrolyte conductivity. Indeed, the pressed electrolyte has higher conductivity than the casted sample (e.g., at 800°C $\sigma_{T\ pressing} = 8.10^{-2}$ S/cm, close to reference values reported in the literature, while $\sigma_{T\ casting} \sim 2.5.10^{-2}$ S/cm in average (depending on the milling conditions, see below). To understand the origin of this difference, the following parameters regarding tape-casting were studied in three successive sections, with the aim to i) find appropriate ball milling tools (jar and balls) avoiding additional pollutions, ii) use different tape-casting organic constituents, and, iii) adjust the debinding conditions.

3.1.1) Effect of the milling media on the chemical pollution of ceria electrolyte obtained by the tape-casting process

Several preliminary experiments were performed in order to prepare dense electrolytes using powders milled during 5h using two materials for jars and balls (alumina or zirconia), as well as involving different milling times. The using of agate was avoided as material milling, because the SiO_2 impurities at the grain boundaries of ceria electrolyte leads to increase the electrical resistivity [14].

The nature of the balls has a large influence on the ionic conductivity of the GDC10 electrolyte: 1.4 x 10^{-2} < σ_T (S/cm) at 800°C < 5.4 x 10^{-2} which, obviously, can be likely due to some pollution during the milling step. For instance, Figure 4 shows a comparison of the ToF-SIMS analysis results obtained on the GDC10 electrolyte made by die pressing (without milling) and by tape casting, which involved a milling step using alumina balls and jar. The alumina pollution in ceria electrolyte due to ball milling formed alumina clusters in the sample, which significantly decreased the total ionic conductivity. The same conclusion was drawn by Nicholas *et al.* regarding 3 mol% Al-doped GDC10 [28]. Alumina then clearly appears as detrimental. Conversely, the possible zirconia pollution associated to the use of milling zirconia balls and jar could not be evidenced by ToF-SIMS, probably because of the solubility of zirconia in ceria (Zr-doped ceria being O^{2-} conductor).

Finally, the conductivity measurements (not shown here) performed on the dense electrolyte prepared after milling steps did not clearly evidence that the couple zirconia jar / zirconia balls will be for sure the best compromise as expected. However, for the following experiments we decided to use them to prepare the suspensions, the optimised milling time being 5h.

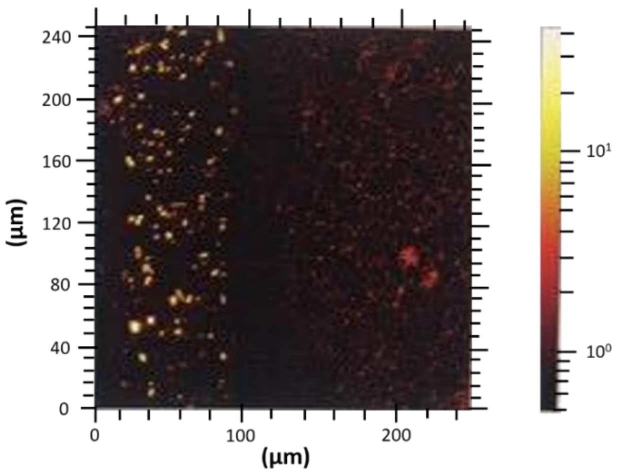

Figure 4: ToF-SIMS analysis of Al in the GDC10 electrolyte obtained by die pressing (on the right) and tape casting with milling by alumina balls (on the left)

3.1.2) Effect of the binder and dispersing agents in the tape-casting suspension on the electrical properties of the GDC10 electrolyte

Table 1 shows the chemical analysis of possible pollutants (Al, Si, Na, K, P) from the organic additives and GDC10 powder in the tape-casting suspension. The organic additives contain notably low concentrations of polluting elements, except for dispersing agents. In particular, dispersing agent C contains larger contents of K (8% wt.), Na (0.08% wt.) and P (6% wt.) than the other two dispersants.

Function	**Chemical nature and references**	**Al (% weight)**	**Si (% weight)**	**Na (% weight)**	**K (% weight)**	**P (% weight)**
Powder	$Ce_{0,9}Gd_{0,1}O_{2-\delta}$	0.14	0.39	< 0.01	< 0.01	< 0.01
Dispersing agent	Phosphate ester (A)	< 0.01	< 0,01	< 0.01	0.02	0.3
	Phosphate ester (B)	< 0.01	< 0,01	0.03	0.01	**3**
	Phosphate ester (C)	< 0.01	< 0.01	**0.08**	**8**	**6**
Plasticizer	Dibutyl phthalate	< 0.01	< 0.01	0.01	0.01	< 0.01
	Polyethylene glycol 200	< 0.01	< 0.01	0.01	0.04	< 0.01
Binder	Polyvinyl Butyral (A: PVB Butyral B90)	0.004	0.004	< 0.01	0.02	< 0.001
	Methyl Methacrylate (B: Degalan LP51/07)	< 0.001	0.004	< 0.001	< 0.001	< 0.001
	Methyl Methacrylate (C)	< 0.001	< 0.001	< 0.001	< 0.001	< 0.001

Table 1: Chemical analysis of different constituents of the tape-casting suspensions obtained by ICP (Inductively Coupled Plasma). The chemical analysis of binders has been performed on ashes obtained after pyrolysis at 400°C for 1 h in air

The impedance diagrams were recorded on GDC10 electrolyte samples, for which the relative density was higher than 94%. An example is shown in Fig. 5. The use of phosphate ester (C) as the dispersant and PVB as the binder leads to the highest total ionic conductivity of GDC10 obtained by tape casting (Figure 6, Table 2). Indeed, the conductivity is similar to that of a pressed pellet as well as that of bibliographic references [14], [29]. Thus, Na, K and P elements (contained in the dispersant) have a low impact on the electrical properties of the GDC10 electrolyte after sintering, at least for T > 500°C. However, in the lowest temperature range (~200°C), the total conductivity of the electrolyte obtained by tape casting remains lower than that obtained by pressing.

Sample	Relative density (%)	σ_T at 800°C (S/cm)	R_{Gb} at 200°C (Ω)
Pressing	97	8.3×10^{-2}	4.0×10^{4}
Tape-casting (B/degalan)	94	2.5×10^{-2}	2.5×10^{7}
Tape-casting (B/PVB)	95	4.8×10^{-2}	9.0×10^{6}
Tape-casting (C/PVB)	94	**7.8×10^{-2}**	**4.7×10^{5}**

Table 2: Effect of the dispersing agents and binders for tape casting with zirconia ball milling on 1) the total conductivity of the GDC10 electrolyte at 800°C and 2) the grain boundaries resistance at 200°C

In Figure 5, on each curve, the left half-circle corresponds to the bulk resistance (f > 10^4 Hz, C ~10^{-10} F), and the right half-circle corresponds to the grain-boundaries resistance (f < 10^4 Hz, 10^{-7} < C (F) < 10^{-8} F). A difference is observed regarding the grain boundary contribution (Table 2): the resistance is maximal for "Tape-casting B/degalan" and minimal for "Tape-casting C/PVB".

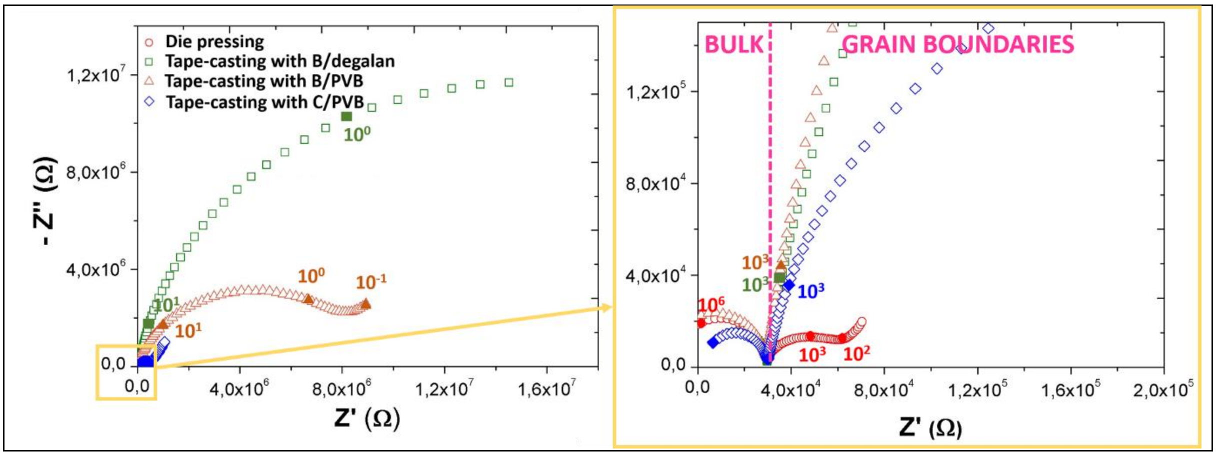

Figure 5: Impedance diagrams recorded at 200°C on symmetrical half-cells, where the electrolyte is prepared by die pressing or tape casting using suspensions with different constituents

Finally, the chemical contamination from the organic components in the tape-casting process may affect the electrical properties of the sintered electrolyte and must be carefully considered. In addition, according to the works by Venkataramana *et al.* [29] and Khan *et al*. [30], [31], ceria-carbonate nano-composites exhibit a multi-ion conduction; then, carbonates can positively contribute to the total ionic conductivity, since carbonates introduce pathways for fast ionic conduction. Carbonates could be present in the as-prepared tape-casted electrolytes. Consequently, at this stage of the study, we must obtain additional data about a possible contribution of carbon on the electrical properties of GDC10.

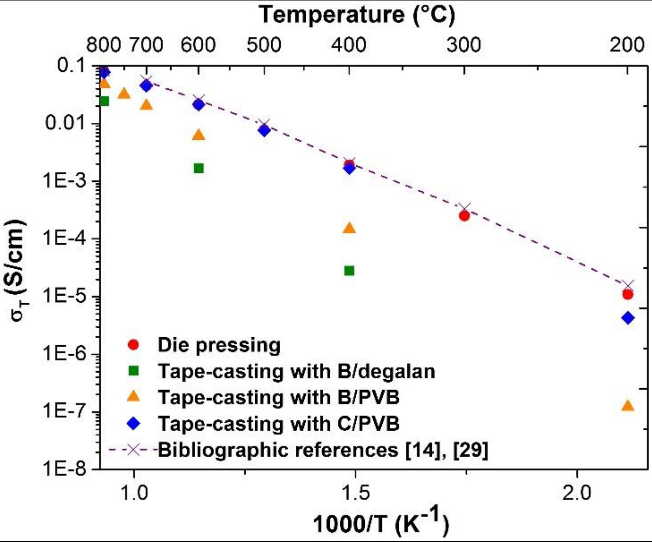

Figure 6: Arrhenius plots of the total conductivity of the GDC10 electrolyte obtained by tape casting using various binders or dispersing agents and milled with zirconia balls. Data from literature ([14], [29]) are added for comparison

3.1.3) Modifications of the electrical properties of the GDC10 electrolyte induced by the carbon contamination during tape casting

Because organic compounds may generate carbon residues during the debinding process, we analysed the samples using Auger Electron Spectroscopy (AES). Chemical analyses were performed in the grains and at the grain boundaries of the dense electrolytes, which were obtained by tape-casting and die pressing.

In the case of samples obtained by die pressing, as expected, no carbon pollution was evidenced in the grains and grain boundaries.

Figures 7a and 7b show fractures of a GDC10 sample obtained by tape casting. This sample is fully dense with some closed pores at the grain boundaries. After etching over a few nanometres to remove the gold metallization, chemical analyses were performed in zone 1, which corresponded to a GDC grain, and zone 2, which corresponded to a grain boundary, as reported in Figures 7c and 7d. During the etching of the grain, the Ce, Gd and O amounts quickly increase over 5-10 nm and subsequently remain steady, which correspond to the chemical composition of GDC10 grains. Finally, no chemical pollution is detected in the GDC10 grains (Figure 7c).

However, even after etching, a large amount of carbon is present at the grain boundary (zone 2) (Figure 7d). This carbon contamination at the grain boundaries likely forms a diffusion barrier to oxygen ions, which induces a decrease in ionic conductivity of the GDC10 material. This carbon contamination at the grain boundaries clearly comes from the burning of organic additives (binder, plasticizer, and dispersing agent) during the debinding step, since it is not observed in the die-pressed samples. Because of the low recorded level of oxygen, we conclude to the absence of carbonates.

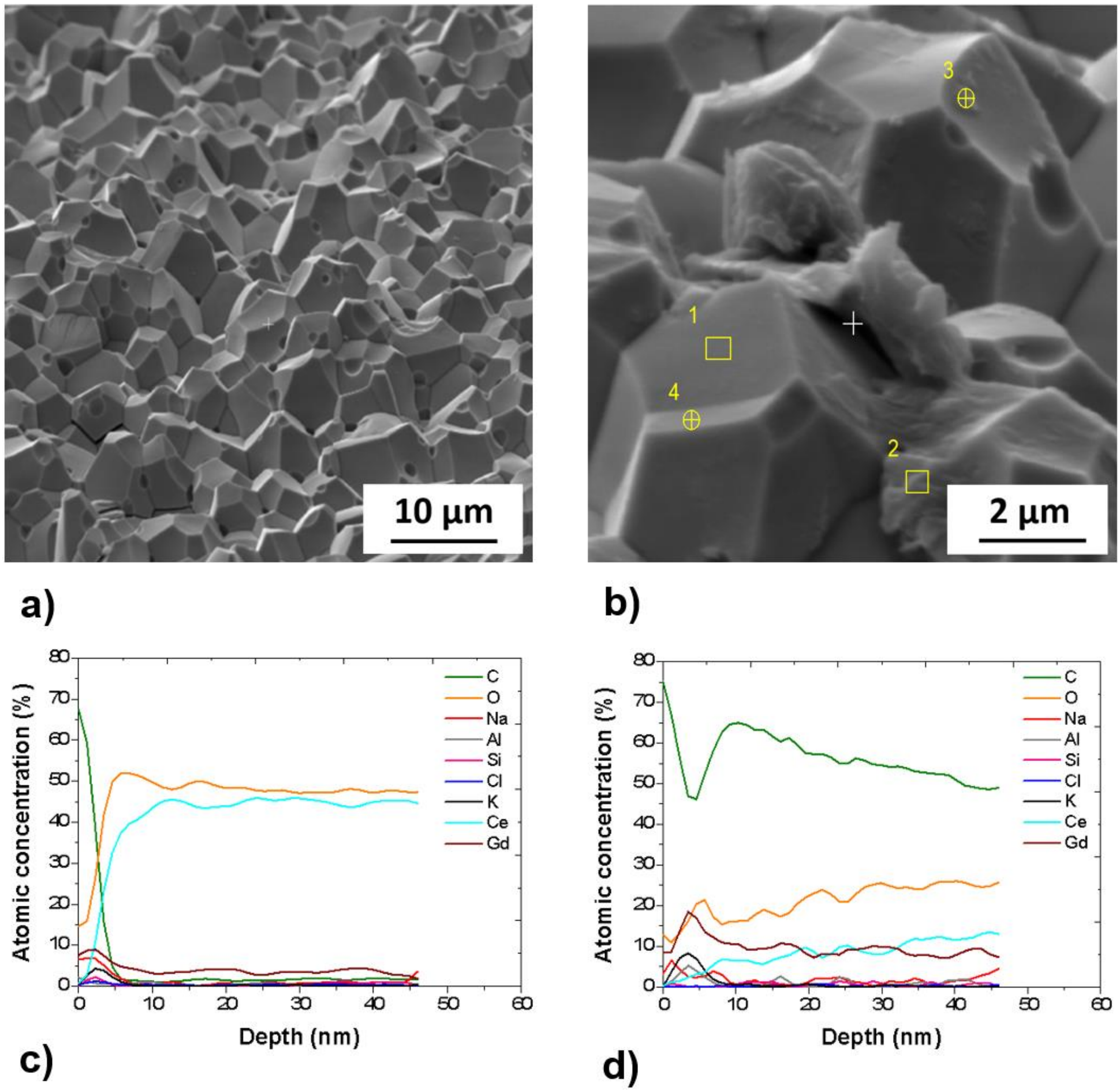

Figure 7: Chemical analysis performed by Auger Electron Spectroscopy (AES) in the grain and at the grain boundaries of GDC10 electrolyte obtained by tape casting: a) b) SEM images, c) analyses on the GDC grain for zone 1 (Fig. 8b) and d) at the grain boundaries for zone 2 (Fig. 8b).

Finally, the carbon contamination in ceria electrolyte segregates at the grain boundary, which increases the grain boundary resistance and decreases the ionic conductivity of ceria electrolyte, particularly at low temperatures (< 400°C, Figure 6). Then, the use of organic additives inherent to the tape-casting process clearly results in a detrimental carbon contamination of the GDC10 electrolyte.

In the remainder of the study, the following constituents of the slurry were selected: phosphate ester C as the dispersing agent and PVB as the binder; milling was performed using zirconia balls and jar.

Indeed, using these constituents leads to the highest conductivity σ_T and lowest grain boundary contribution (Table 2).

3.2) Characterization of tape-casted/impregnated symmetrical SOCs by EIS

In order to remove the residual carbon pollution located at grain boundaries, we aimed to modify the debinding cycle including the surrounding atmosphere. The corresponding modifications of the ionic conductivity of ceria electrolyte are studied in this section.

Three debinding processes were successively tested on symmetrical oxygen side cells made by tape casting:

- (1) debinding under air flow at 800°C during 2 h (Tape casting 1)
- (2) debinding under dry O_2 flow at 800°C during 6 h (Tape casting 2)
- (3) debinding under wet O_2 flow at 800°C during 6 h (Tape casting 3). For this purpose, oxygen gas was simply introduced by a bubbler system containing water at the entrance of the furnace, which corresponds to a partial pressure of water near 2.5 10^{-2} atm (one/two litres of gas per hour).

We aimed to compare debinding under air and oxygen flows with the expectation to increase the carbon departure in the CO_2 form in the second case. Moreover, in the last case (3), the addition of steam water in the oxygen flow promotes the carbon removal due to the water gas shift reaction, according to ref. [32].

The objective was to obtain a symmetrical cell made by tape casting after the impregnated steps, which has similar electrochemical performances to a die-pressed/screen-printed one. Thus, at the same temperature, the electrolyte must be dense, and the backbones must be sufficiently porous to enable efficient infiltration, which is a challenging task. The temperature was optimized through impedance measurements with SEM observations; finally, the most suitable temperature was 1450°C. The electrolyte density appears slightly lower than 95% at least according to the observations, which can partly decrease the conductivity of the electrolyte. In Figure 8, images of sections recorded on a symmetrical infiltrated support either prepared by die-pressing/screen-printing (Figure 8.a) or by tape-casting (Figure 8.b) are shown. In the first case, Pr_6O_{11} homogeneously covers the porous GDC skeleton, while in the second case it is more localized in the grain boundaries. Moreover, the GDC grain size of the casted sample is larger than that of the screen-printed one.

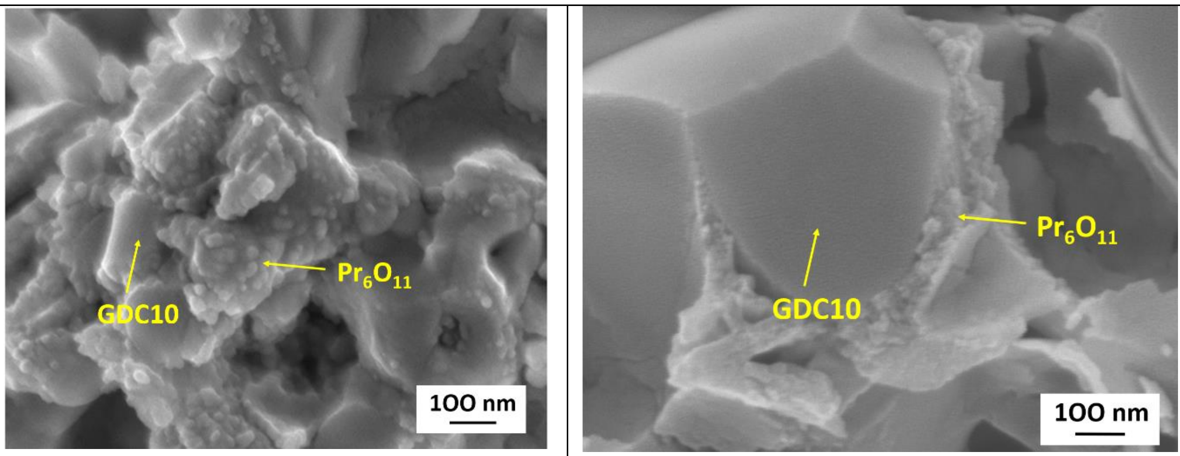

a) b)

Figure 8 – Images of sections showing Pr_6O_{11} infiltration in a) die-pressed / screen-printed sample, b) tape-casted sample

Fig. 9 shows the thermal variation of the polarization resistance for cells made by tape casting according to the three debinding treatments. The best performances were obtained by debinding under dry and subsequently wet O_2 (Tape casting 3). This debinding treatment is then favourable to remove carbon in the ceria electrolyte. It is assumed here that the carbon contamination at grain boundaries of ceria electrolyte leads to a decrease of the ionic conductivity as well as an increase of the electrode polarisation resistance.

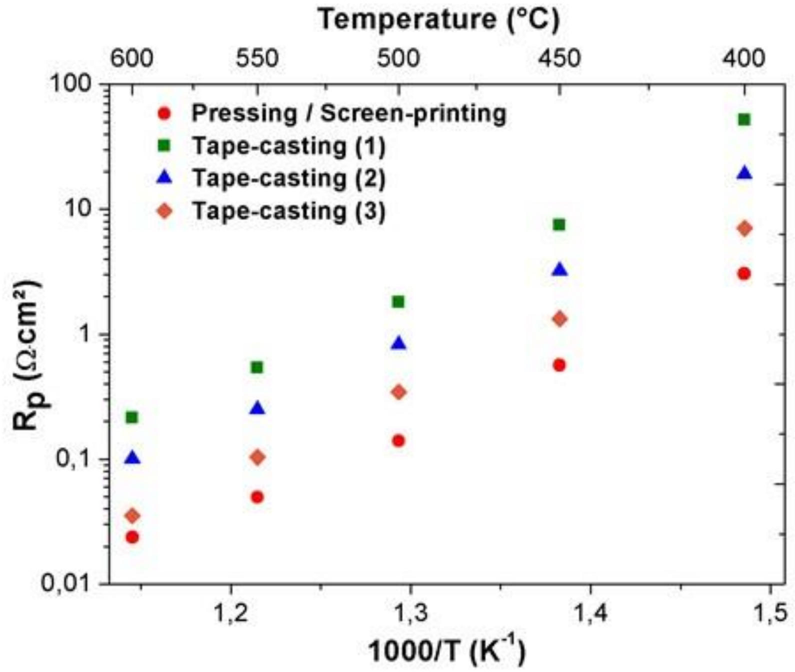

Figure 9: Arrhenius plots of R_p for impregnated symmetrical oxygen side cells made by tape casting according to various debinding processes in comparison with the pressed/screen-printed cells.

Despite an improvement of the electrochemical performances of the casted sample thanks to an improved debinding process, there are still a bit lower than those of the die-pressed / screen-printed sample (Figure 9). This observation could be explained by the difference regarding the infiltration results as detailed above.

4) **Conclusion**

Symmetrical cells with GDC10 electrolyte and a specific design (porous/dense/porous) have been produced by tape casting. This shaping process allows elaborating the cells in one-step with an accurate thickness control and an improved interface quality between the electrolyte and the electrodes. The porous electrodes are subsequently infiltrated by a precursor of the catalyst followed by a thermal treatment at low temperature. The process parameters must be carefully adjusted; in particular, the choice of milling media and organic additives is important to avoid contaminating the material, and the operating conditions of debinding are important to remove all carbon residues. These parameters directly affect the final ionic conductivity of the GDC10 electrolyte and the polarization resistance of the symmetrical cell infiltrated with Pr_6O_{11}. The debinding performed under oxygen and/or water steam improves the removal of carbon residues at the grain boundaries.

The next step has been to optimize the sintering temperature of the tape-casted porous/dense/porous GDC10 architecture through impedance measurements and SEM observations; an almost fully dense electrolyte and sufficiently porous backbones for efficient infiltration has been obtained. The polarization resistances of such optimized and impregnated symmetrical (oxygen side) cells are close to those of the corresponding ones elaborated by die-pressing/screen-printing.

Finally, we have shown that a one-step process that obviously reduces manufacturing costs, provides solutions for improving the electrochemical properties of SOCs. A future work will be the preparation of a complete cell by tape casting, including a thin electrolyte membrane ($\approx$ 10-20 µm) layered on a thick hydrogen-side porous support ($\approx$ 200 µm).

Acknowledgements

This research was partly supported by a French regional fellowship "*Région Nouvelle Aquitaine*" (for L.G.). LG, JCG and JMB are grateful for the financial support obtained through the ANR project ECOREVE (ANR-18-CE05-0036-01). All authors acknowledge the French group GDR HysPac for fruitful discussions. Finally, the authors are grateful to the Solvay company (France) for providing the chemical precursors and powders employed in this work.

References

[1] J. B. Goodenough, « Oxide-Ion Electrolytes », *Annual Review of Materials Research*, vol. 33, n° 1, p. 91-128, 2003.

[2] B. C. H. Steele et A. Heinzel, « Materials for fuel-cell technologies », *Nature*, p. 345-352, 2001.

[3] R. Knibbe, A. Hauch, J. Hjelm, S. D. Ebbesen, et M. Mogensen, « Durability of Solid Oxide Cells », *Green*, p. 141-199, 2011.

[4] J. Schefold, A. Brisse, et F. Tietz, « Nine Thousand Hours of Operation of a Solid Oxide Cell in Steam Electrolysis Mode », *Journal of the Electrochemical Society*, p. A137-A144, 2012.

[5] Q. Fang, L. Blum, et N. H. Menzler, « Performance and Degradation of Solid Oxide Electrolysis Cells in Stack », *Journal of the Electrochemical Society*, p. F907-F912, 2015.

[6] J.-H. Lee *et al.*, « Degradation Mechanism of Oxygen Electrode Under Fuel-Cell and Electrolysis Mode Operations », *ECS Trans.*, vol. 91, n° 1, p. 681-685, 2019.

[7] Q. Fang, L. Blum, et D. Stolten, « Electrochemical Performance and Degradation Analysis of an SOFC Short Stack for Operation of More than 100,000 Hours », *ECS Trans.*, vol. 91, n° 1, p. 687-696, 2019.

[8] Q. Fang, C. E. Frey, N. H. Menzler, et L. Blum, « Electrochemical Performance and Preliminary Post-Mortem Analysis of a Solid Oxide Cell Stack with 20,000 h of Operation », *Journal of the Electrochemical Society*, p. F38-F45, 2018.

[9] Y. Tian, H. Zheng, L. Zhang, B. Chi, J. Pu, et J. Li, « Direct Electrolysis of CO2 in Symmetrical Solid Oxide Electrolysis Cell Based on La0.6Sr0.4Fe0.8Ni0.2O3-δ Electrode », *Journal of the Electrochemical Society*, p. F17-F23, 2018.

[10] Y. F. Tian *et al.*, « Preparation and Performance of Sr-Co Free Perovskite-Type Oxide La0.6Ca0.4Fe0.8Ni0.2O3-δ as an Oxygen Electrode for Reversible Solid Oxide Electrochemical Cell », *ECS Transactions*, vol. 91, n° 1, p. 2351-2358, 2019.

[11] J. Railsback, S. H. Choi, et S. A. Barnett, « Effectiveness of dense Gd-doped ceria barrier layers for (La,Sr)(Co,Fe)O3 cathodes on Yttria-stabilized zirconia electrolytes », *Solid State Ionics*, vol. 335, p. 74-81, 2019.

[12] R. Kiebach *et al.*, « Stability of La 0.6 Sr 0.4 Co 0.2 Fe 0.8 O 3 /Ce 0.9 Gd 0.1 O 2 cathodes during sintering and solid oxide fuel cell operation », *Journal of Power Sources*, vol. 283, p. 151-161, 2015.

[13] T. Matsui, S. Li, Y. Inoue, N. Yoshida, H. Muroyama, et K. Eguchi, « Degradation Analysis of Solid Oxide Fuel Cells with (La,Sr)(Co,Fe)O3-δ cathode/Gd2O3–CeO2 Interlayer/Y2O3–ZrO2 Electrolyte System: The Influences of Microstructural Change and Solid Solution Formation », *ECS Transactions*, vol. 91, p. 1247-1256, 2019.

[14] B. C. H. Steele, « Appraisal of Ce1-yGdyO2y/2 electrolytes for IT-SOFC operation at 500°C », *Solid State Ionics*, p. 95-100, 2000.

[15] A. Atkinson *et al.*, « Advanced anodes for high-temperature fuel cells », *Nature materials*, vol. 3, p. 17-27, 2004.

[16] J. M. Vohs et R. J. Gorte, « High-Performance SOFC Cathodes Prepared by Infiltration », *Advanced Materials*, p. 943-956, 2009.

[17] A. Samson, M. Sogaard, R. Knibbe, et N. Bonanos, « High Performance Cathodes for Solid Oxide Fuel Cells Prepared by Infiltration of La 0.6 Sr 0.4 CoO 32d into Gd-Doped Ceria », *Journal of the Electrochemical Society*, p. B650-B659, 2011.

[18] P. V. Hendriksen, M. Khoshkalam, K. Tong, D. Tripkovic, M. A. Faghihi-Sani, et M. Chen, « Improving oxygen electrodes by infiltration and surface decoration », *The Electrochemical Society*, p. 1413-1424, 2019.

[19] D. Ding, X. Li, S. Y. Lai, K. Gerdes, et M. Liu, « Enhancing SOFC cathode performance by surface modification through infiltration », *Energy Environ. Sci.*, vol. 7, n° 2, p. 552, 2014.

[20] S. P. Jiang, « A review of wet impregnation—An alternative method for the fabrication of high performance and nano-structured electrodes of solid oxide fuel cells », *Materials Science and Engineering: A*, vol. 418, n° 1-2, p. 199-210, 2006.

[21] M. Shah et S. Barnett, « Solid oxide fuel cell cathodes by infiltration of La0.6Sr0.4Co0.2Fe0.8O3−δ into Gd-Doped Ceria », *Solid State Ionics*, vol. 179, n° 35-36, p. 2059-2064, 2008.

[22] C. Nicollet, A. Flura, V. Vibhu, A. Rougier, J.-M. Bassat, et J.-C. Grenier, « An innovative efficient oxygen electrode for SOFC: Pr_6O_{11} infiltrated into Gd-doped ceria backbone », *International Journal of Hydrogen Energy*, p. 15538-15544, 2016.

[23] K. Vidal, A. Moran-Ruiz, J. M. Porras-Vasquez, P. R. Slater, et M. I. Arriortua, « Characterization of LaNi 0.6 Fe 0.4 O 3 perovskite synthesized by glycine-nitrate combustion method », *Solid State Ionics*, p. 24-29, 2014.

[24] J. Kiennemann, « Comportement dans l'eau d'alumines issues du procédé Bayer : Application au coulage en bande en milieu aqueux », Université de Limoges, 2004.

[25] T. Chartier et P. Boch, « Matériaux et processus céramiques », *Hermes Science Publications*, 2001.

[26] T. Chartier, « Tape Casting », in *The Encyclopedia of Advanced Materials*, Pergamon Press., 1973, p. 2763.

[27] A. Flura *et al.*, « Application of the Adler-Lane-Steele model to porous La2NiO4+δ SOFC cathode : influence of interfaces with gadolinia doped ceria », *Journal of the Electrochemical Society*, vol. 163, n° 6, p. F523-F532, 2016.

[28] J. D. Nicholas et L. C. De Jonghe, « Prediction and evaluation of sintering aids for Cerium Gadolinium Oxide », *Solid State Ionics*, p. 1187-1194, 2007.

[29] B. Dalslet, P. Blennow, P. Vang Hendriksen, N. Bonanos, D. Lybye, et M. Mogensen, « Assessment of doped ceria as electrolyte », *Journal of Solid State Electrochemical*, p. 547-561, 2006.

[30] K. Venkataramana, C. Madhuri, et C. V. Reddy, « Enhanced ionic conductivity of co-doped ceria-carbonate nano composite electrolyte material for LT-SOFCs », *DAE Solid State Physics Symposium*, p. 0500241-0500243, 2017.

[31] I. Khan, M. I. Asghar, P. D. Lund, et S. Basu, « High conductive (LiNaK)2CO3-Ce0.85Sm0.15O2 electrolyte compositions for IT-SOFC applications », *International Journal of Hydrogen Energy*, p. 20904-20909, 2017.

[32] I. Khan, P. K. Tiwari, et S. Basu, « Development of melt infiltrated gadolinium doped ceria-carbonate composite electrolytes for intermediate temperature solid oxide fuel cells », *Electrochimica Acta*, p. 1-10, 2019.

[33] E. Obeid, « Catalyseurs conducteurs ioniques pour l'oxydation des suies », Université de Lyon, 2013.